AGU PUBLICATIONS

JGR

Journal of Geophysical Research: Space Physics

RESEARCH ARTICLE
10.1002/2015JA021563

Key Points:
- Chorus emissions can accelerate electrons from tens of keV to several MeV within a few minutes
- A dumbbell distribution of relativistic electrons is formed by nonlinear trapping (RTA + URA)
- A numerical Green's function method for chorus wave-particle interaction is formulated

Correspondence to:
Y. Omura,
omura@rish.kyoto-u.ac.jp

Citation:
Omura, Y., Y. Miyashita, M. Yoshikawa, D. Summers, M. Hikishima, Y. Ebihara, and Y. Kubota (2015), Formation process of relativistic electron flux through interaction with chorus emissions in the Earth's inner magnetosphere, *J. Geophys. Res. Space Physics*, *120*, 9545–9562, doi:10.1002/2015JA021563.

Received 10 JUN 2015
Accepted 19 OCT 2015
Accepted article online 17 NOV 2015
Published online 21 NOV 2015

Formation process of relativistic electron flux through interaction with chorus emissions in the Earth's inner magnetosphere

Yoshiharu Omura[1], Yu Miyashita[1], Masato Yoshikawa[1], Danny Summers[1,2], Mitsuru Hikishima[1,3], Yusuke Ebihara[1], and Yuko Kubota[1]

[1]Research Institute for Sustainable Humanosphere, Kyoto University, Uji, Japan, [2]Department of Mathematics and Statistics, Memorial University of Newfoundland, St. John's, Newfoundland and Labrador, Canada, [3]Institute of Space and Astronautical Science, Japan Aerospace Exploration Agency, Sagamihara, Japan

Abstract We perform test particle simulations of energetic electrons interacting with whistler mode chorus emissions. We compute trajectories of a large number of electrons forming a delta function with the same energy and equatorial pitch angle. The electrons are launched at different locations along the magnetic field line and different timings with respect to a pair of chorus emissions generated at the magnetic equator. We follow the evolution of the delta function and obtain a distribution function in energy and equatorial pitch angle, which is a numerical Green's function for one cycle of chorus wave-particle interaction. We obtain the Green's functions for the energy range 10 keV–6 MeV and all pitch angles greater than the loss cone angle. By taking the convolution integral of the Green's functions with the distribution function of the injected electrons repeatedly, we follow a long-time evolution of the distribution function. We find that the energetic electrons are accelerated effectively by relativistic turning acceleration and ultrarelativistic acceleration through nonlinear trapping by chorus emissions. Further, these processes result in the rapid formation of a dumbbell distribution of highly relativistic electrons within a few minutes after the onset of the continuous injection of 10–30 keV electrons.

1. Introduction

Electromagnetic whistler mode emissions known as chorus have been extensively observed in Earth's inner magnetosphere [e.g., *Tsurutani and Smith*, 1974; *Koons and Roeder*, 1990; *Meredith et al.*, 2001, 2014; *Santolik et al.*, 2008, 2014; *Spasojevic*, 2014]. Chorus typically comprises coherent rising tone emissions generated near the magnetic equator. The chorus generation mechanism is the electron cyclotron resonance instability resulting from an anisotropic distribution of (~10 keV) electrons injected from the plasma sheet region during geomagnetically disturbed times [*Omura et al.*, 1991; *Nunn et al.*, 1997]. Chorus plays a key role in radiation belt dynamics in at least two respects. First, chorus is a generator of relativistic (MeV) electrons that replenish Earth's outer radiation belt [*Summers et al.*, 1998, 2002, 2007; *Varotsou et al.*, 2005; *Mourenas et al.*, 2012; *Thorne et al.*, 2013; *Xiao et al.*, 2014; *Su et al.*, 2014; *Li et al.*, 2014; *Liu et al.*, 2015]. Second, chorus can pitch angle scatter electrons into the atmospheric loss cone, thereby resulting in the depletion of electrons from the outer zone [*Lorentzen et al.*, 2001; *O'Brien et al.*, 2004; *Thorne et al.*, 2005; *Summers et al.*, 2007, 2009; *Shprits et al.*, 2007; *Tsurutani et al.*, 2009; *Lakhina et al.*, 2010; *Hikishima et al.*, 2010a; *Boynton et al.*, 2014; *Summers and Shi*, 2014; *Harid et al.*, 2014]. In the present investigation, we analyze the acceleration of electrons to relativistic energies by chorus, using a particle simulation that takes into account the appropriate nonlinear physics that has typically been excluded from most previous simulations.

Omura and Summers [2006] presented a test particle simulation demonstrating that a fraction of weakly relativistic electrons can be trapped by a coherent chorus wave and that the trapped electrons are effectively accelerated by a rising tone chorus element. *Omura et al.* [2007] reported a very efficient relativistic electron acceleration mechanism by a long-time whistler mode wave packet, in which electrons are accelerated to a few MeV through a single resonant trapping process. We named this particular acceleration process "relativistic turning acceleration (RTA)." *Summers and Omura* [2007] showed that MeV electrons are further accelerated to higher energy by a special form of nonlinear phase trapping by a coherent whistler mode wave, in which both relativistic electrons and wave packets are moving in the same direction.

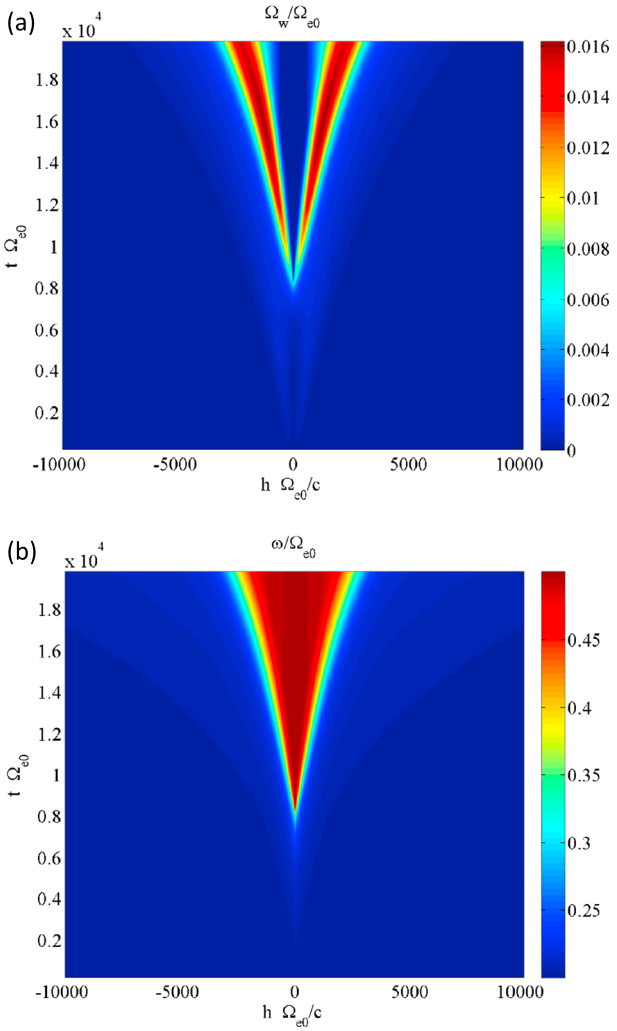

Figure 1. Spatial and temporal evolutions of (a) wave amplitude and (b) frequency of a pair of chorus elements obtained by solving the chorus equations and the wave equations. The chorus wave packets are generated at the equator starting from an amplitude $\Omega_w = 0.0005\Omega_{e0}$ and a frequency $\omega = 0.2\Omega_{e0}$. When the wave frequency reaches $\omega = 0.5\Omega_{e0}$, the wave packets are terminated at the equator, and they propagate away from the equator, undergoing convective wave growth.

This acceleration process is called "ultra-relativistic acceleration (URA)." *Katoh and Omura* [2007a] used an electron hybrid simulation to reproduce chorus emissions growing from thermal noise and forming coherent rising tone emissions. *Hikishima et al.* [2009, 2010a, 2010b] also performed electromagnetic particle simulations reproducing chorus emissions and associated nonlinear pitch angle scattering, resulting in electron microbursts. Chorus wave growth is due to the formation of electron holes in the velocity phase space due to nonlinear trapping by coherent wave potentials [*Omura et al.*, 2008, 2009, 2012]. *Katoh and Omura* [2007b] confirmed that the RTA process takes place in a self-consistent particle simulation reproducing chorus emissions. *Furuya et al.* [2008] presented a series of test particle simulations reproducing a high-energy tail in the electron energy distribution function via RTA. A Green's function of kinetic energy for chorus wave-particle interaction was developed in their study, and the present study is an extension of the method to include the dependency on equatorial pitch angles.

In section 2 we describe a model of chorus elements that interact with energetic electrons near the magnetic equator, and we present two cases of efficient acceleration of energetic electrons. We develop in section 3 a numerical Green's function method in which the Green's function specifies the energy and equatorial pitch angle for the nonlinear wave-particle interactions with chorus emissions. In section 4, we solve the relativistic equations of motion for many particles under the influence of the chorus elements to obtain each of the Green's functions for different combinations of energy and equatorial pitch angle. In section 5, we follow long-time evolutions of the distribution function in the (energy and pitch angle) phase space by carrying out a numerical convolution integral with the Green's functions. Finally, we present a summary and discussion in section 6.

2. Test Particle Simulation With Model of Chorus Elements

We first set up a model of a chorus element, i.e., a single rising tone emission based on the "chorus equations" [*Omura et al.*, 2009] at the equator, and obtain the spatial and temporal variation of the chorus wave field by integrating the wave equations [*Omura et al.*, 2008] in space and time. This technique is based on the method developed by *Summers et al.* [2012], where an adiabatic variation of the energetic electrons is assumed in the calculation of the resonant current parallel to the wave electric field. Since the generation of chorus elements takes place in both northward and southward directions at the equator, we assume a pair of chorus elements with the same wave properties but propagating in opposite directions. The spatial and temporal evolution

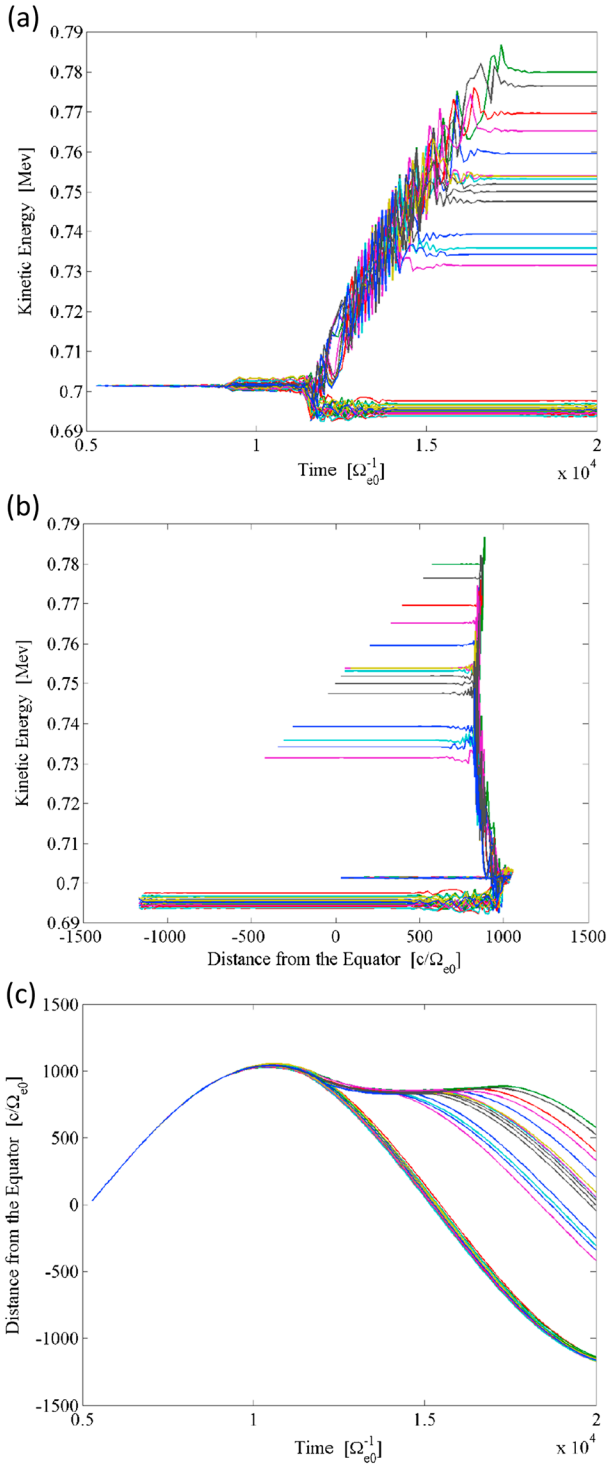

Figure 2. Trajectories of resonant electrons undergoing relativistic turning acceleration (RTA). Electrons are started with the same velocity and different gyrophases. In approaching the equator after being reflected back from the mirror point, some of the electrons are trapped by the wave potential and they change their direction of motion. (a) Kinetic energies as functions of time. (b) Kinetic energies as functions of distance. (c) Locations along the magnetic field line plotted as functions of time.

of the wave amplitude and frequency of the chorus elements are shown in Figures 1a and 1b, respectively. We normalize the distance along the magnetic field line by c/Ω_{e0}, where c and Ω_{e0} are the speed of light and the electron cyclotron frequency Ω_e at the equator, respectively. The wave amplitude B_w is normalized as $\Omega_w = eB_w/m_e$, where e and m_e are the charge and rest mass of an electron. The spatial length of the simulation model must be taken large enough so as to accommodate the bounce motions of all resonant electrons trapped in the assumed model of the Earth's dipole magnetic field. We assume a dipole magnetic field at $L = 4.5$, background plasma frequency $\omega_{pe} = 4\Omega_{e0}$, plasma frequency of hot electrons $\omega_{ph} = 0.2828\Omega_{e0}$, depth of electron hole $Q = 0.5$, average perpendicular velocity $V_{\perp 0} = 0.3c$, parallel thermal momentum $U_{t\|} = 0.15c$, parabolic coefficient of the dipole magnetic field $a = 2.3 \times 10^{-7}\Omega_{e0}^2/c^2$ defined by $\Omega_e(h) = \Omega_{e0}(1 + ah^2)$, and the initial wave amplitude $\Omega_w = 0.0005\Omega_{e0}$. Detailed descriptions of these variables are given in *Summers et al.* [2012]. With these parameters, the chorus wave packets reach the maximum amplitude $\Omega_w = 0.015\Omega_{e0}$, which corresponds to 5 nT. Recent observations by the Van Allen Probes show that there do exist such large-amplitude chorus wave packets [*Santolik et al.*, 2014].

To calculate the motion of test particles interacting with the chorus waves, we solve the relativistic equation of motion in the presence of the electromagnetic field of the chorus waves propagating along the dipole field line. The numerical method of solving the trajectories of electrons is described in *Omura and Summers* [2006]. In the computation of the wave fields, we used 500 grid points with a grid spacing $\Delta h = 40c/\Omega_{e0}$. Because of the symmetry of the wave packets in the Northern and Southern Hemispheres, we only inject electrons moving northward initially with positive velocities. The trajectories of electrons are followed with a time step $\Delta t = 0.02\Omega_{e0}^{-1}$ until $t = 30{,}000\Omega_{e0}^{-1}$.

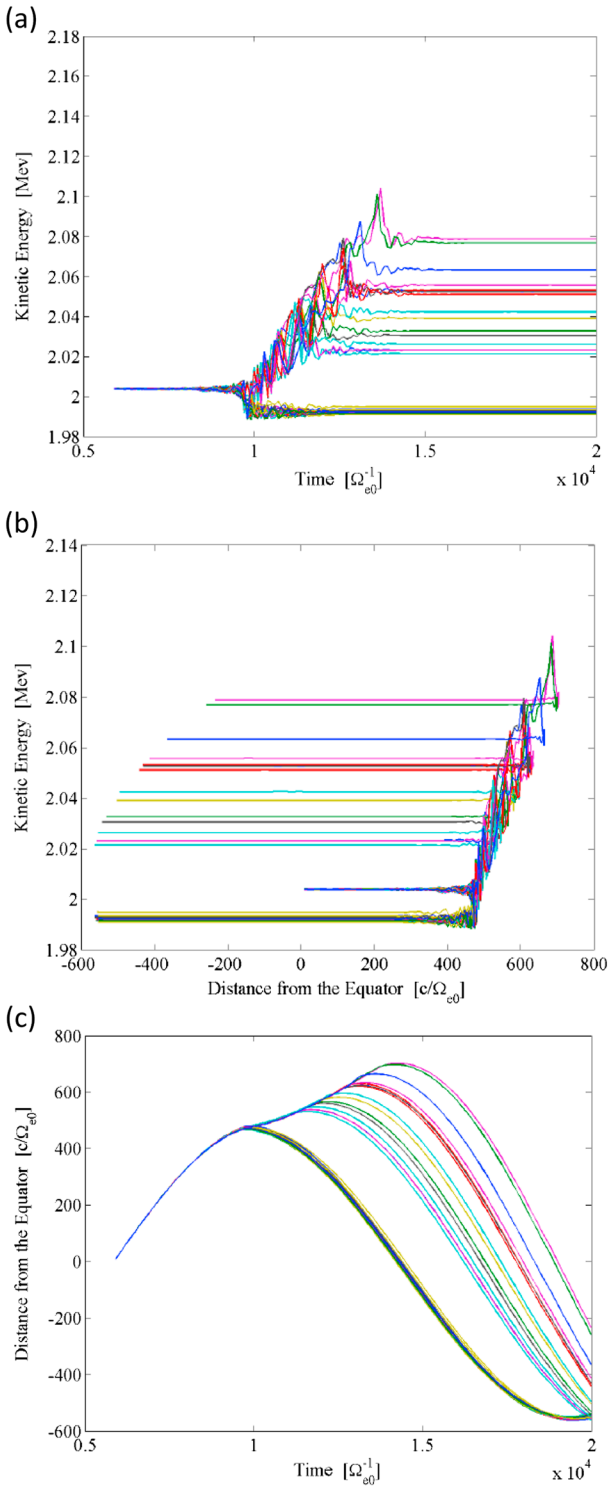

Figure 3. Trajectories of resonant electrons undergoing ultrarelativistic acceleration (URA). Electrons are started with the same velocity and different gyrophases. In moving away from the equator, some of the electrons are trapped by the wave potential and are accelerated effectively. (a) Kinetic energies as functions of time. (b) Kinetic energies as functions of distance. (c) Locations along the magnetic field line plotted as functions of time.

Effective acceleration of electrons takes place for resonant electrons trapped by the wave. We traced trajectories of energetic electrons of 0.7 MeV injected with a positive parallel velocity near the resonance velocity, a perpendicular velocity, and different gyrophases. The kinetic energies of the particles as functions of time t and distance h are plotted in Figures 2a and 2b, respectively. The positions of the particles are also plotted as functions of time in Figure 2c. Figure 2a shows that the resonant electrons are divided into two groups depending on their phases relative to the wave phase. Some of these are trapped by the wave, and efficiently accelerated, while others lose energy slightly at the resonance, then continuing on adiabatic trajectories. Figures 2b and 2c indicate that the trapped resonant electrons remain in a given hemisphere while they are accelerated. The electrons change their motion from the negative to positive directions due to the change in sign of the resonance velocity. This is a typical example of relativistic turning acceleration (RTA) [*Omura et al.*, 2007].

In Figure 3 we show another example of electron trajectories, here with 2 MeV electrons. Figure 3a shows that electrons trapped by the wave are accelerated, while those untrapped lose a small amount of energy to the wave through the resonance. Figures 3b and 3c show that some of the electrons are trapped by the wave at $h = 470c/\Omega_{e0}$ and $t = 10{,}000\Omega_{e0}^{-1}$ while moving away from the equator, being accelerated effectively. Some of the trapped electrons are gradually detrapped in time, undergoing adiabatic motions. The acceleration in the energy range greater than 1 MeV ($\gamma > \Omega_e/\omega$) takes place when the electrons are moving in the same direction as the wave packet. The acceleration through nonlinear trapping by the wave packet takes a longer time than the case of lower energy electrons counterstreaming against the wave packet. This form of efficient acceleration is called ultrarelativistic acceleration (URA) [*Summers and Omura*, 2007].

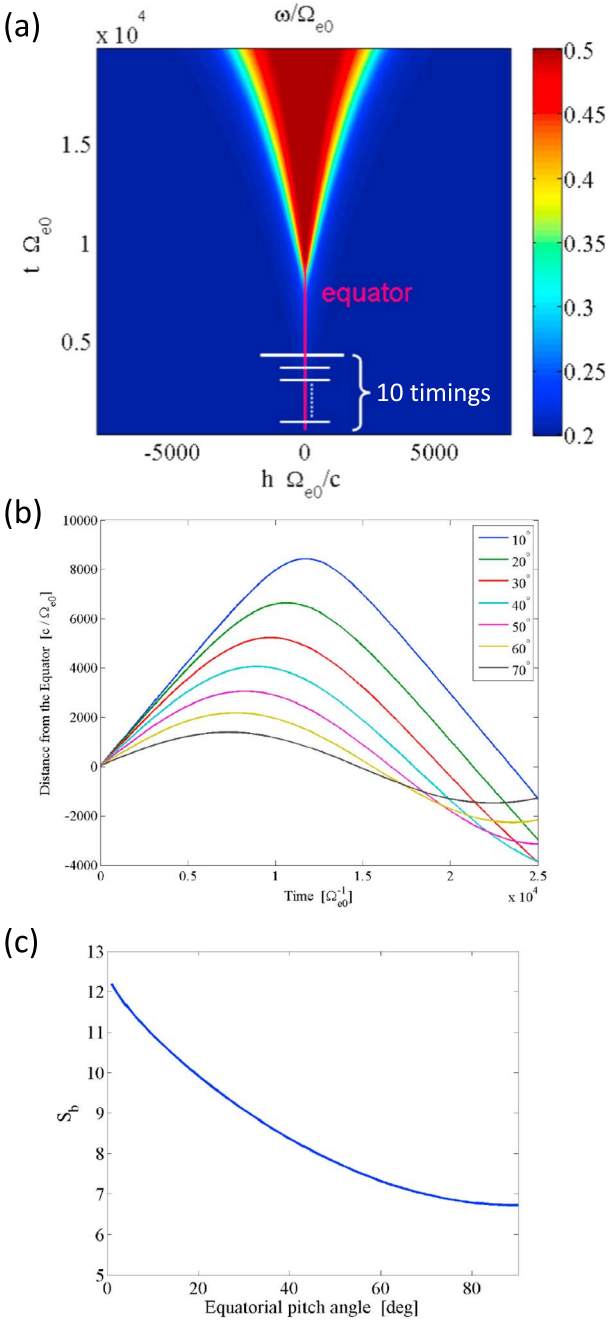

Figure 4. (a) Timings of electron injections with respect to the evolution of the wave frequency in space and time. For the calculation of each Green's function $G(E, E_1, \alpha, \alpha_1)$, 3600 electrons are injected with different combinations of 36 gyrophases, at 10 locations between the equator and the mirror point, and 10 injection timings. (b) Adiabatic trajectories of electrons with different equatorial pitch angles. All electrons are injected with positive parallel velocities. (c) Bounce motion factor S_b as a function of the equatorial pitch angle.

3. Numerical Green's Function Method

We assume a distribution function of kinetic energy E and pitch angle α_{eq} at the magnetic equator. Since energetic electrons trapped by the dipole magnetic field undergo adiabatic mirror motion, the distribution function $f(E, \alpha_{eq})$ represents all energetic electrons at different locations along a magnetic field line with energy E and equatorial pitch angle α_{eq}. The pitch angle α at a distance h from the equator along the magnetic field is given by

$$\alpha(h) = \arcsin\left(\sqrt{\frac{B(h)}{B_{eq}}}\sin\alpha_{eq}\right). \quad (1)$$

In calculating the time evolution of the distribution function through interaction with a pair of chorus wave packets described in the previous section, we need to solve the motions of energetic particles injected at different locations and timings of the wave packet evolution as shown in Figure 4a. This is so that the distribution should represent the bounce-averaged distribution correctly.

To evaluate the evolution of the bounce-averaged distribution function, we must take into account the variation of the phase space volume element dV when the particles are scattered in energies and pitch angles. The total number of test particles N has to correspond to the volume integral of the electron distribution function f with respect to dV, namely,

$$N = \int f dV \,. \quad (2)$$

Figure 4b shows the adiabatic trajectories of the electrons in the dipole magnetic field. As we find in Figure 4b, the bounce path lengths of electrons trapped in the dipole field depend on their pitch angles. Therefore, we have to evaluate the bounce path lengths when we calculate dV. We adopt the analysis method of the bounce path length based on *Jordanova et al.* [1996]. The momentum of an electron is given by

$$p = \frac{\sqrt{E^2 + 2m_e c^2 E}}{c} \,. \quad (3)$$

When the first adiabatic invariant is conserved, the perpendicular and parallel components of the momentum at a given position are given by

$$p_\perp = p\sqrt{\frac{B(h)}{B_{eq}}\left(1-\cos^2\alpha_{eq}\right)} \tag{4}$$

and

$$p_\parallel = p\sqrt{1-\frac{B(h)}{B_{eq}}\left(1-\cos^2\alpha_{eq}\right)}\ , \tag{5}$$

where B_{eq} and $B(h)$ are the magnetic field at the equator and the magnetic field at the position h, respectively. The Jacobian transformation is then given by

$$\frac{\partial(p_\perp, p_\parallel)}{\partial(E, \cos\alpha_{eq})} = m_e\gamma\left(1-\frac{B(h)}{B_m}\right)^{-1/2}\frac{B(h)}{B_{eq}}\frac{p}{p_\perp}\cos\alpha_{eq}\ , \tag{6}$$

where B_m denotes the magnetic field at the mirror point. By following *Jordanova et al.* [1996], the volume element dV is given by

$$dV = d^3\boldsymbol{r}\,d^3\boldsymbol{p} = 4\pi p_\perp dp_\perp dp_\parallel \frac{B_{eq}}{B(h)}R_{eq}dR_{eq}d\phi dh\,, \tag{7}$$

where R_{eq} is the radial distance at the equator and ϕ is the longitudinal angle. Taking (6) into consideration, we obtain the relation

$$dV = -4\pi m_e\gamma\left(1-\frac{B(h)}{B_m}\right)^{-1/2} p\sin\alpha_{eq}\cos\alpha_{eq}dEd\alpha_{eq}R_{eq}dR_{eq}d\phi dh\ . \tag{8}$$

We assume that energetic electrons only move along the magnetic field line during the time of resonant interaction with the waves. Integrating (8) over the distance h along the magnetic field line between the mirror points $\pm h_m$, we obtain

$$dV_m = -4\pi m_e S_b(R_{eq}, \cos\alpha_{eq})\gamma p\sin\alpha_{eq}\cos\alpha_{eq}dEd\alpha_{eq}R_{eq}dR_{eq}d\phi\ , \tag{9}$$

where S_b is the function given by

$$S_b = \int_{-h_m}^{h_m}\left(1-\frac{B(h)}{B_m}\right)^{-\frac{1}{2}}dh\ . \tag{10}$$

The variation of S_b as a function of equatorial pitch angle is plotted in Figure 4c. We define the phase space volume of trapped electrons over a unit area of the cross-section $R_{eq}dR_{eq}d\phi$ of the flux tube as $dV_{mu} = -A(E, \alpha_{eq})dEd\alpha_{eq}$, where

$$A(E, \alpha_{eq}) = 4\pi m_e\gamma S_b(R_{eq}, \cos\alpha_{eq})p\sin\alpha_{eq}\cos\alpha_{eq}\ . \tag{11}$$

Expressing γ and p in terms of the kinetic energy E, we obtain

$$A(E, \alpha_{eq}) = 2\pi m_e^{3/2}E^{1/2}\left(1+\frac{E}{m_ec^2}\right)\left(2+\frac{E}{m_ec^2}\right)^{1/2}S_b(R_{eq}, \alpha_{eq})\sin 2\alpha_{eq}\ . \tag{12}$$

In the following we omit the subscript "eq" of α, and the pitch angle α henceforth means the equatorial pitch angle. When a test particle with the phase space density f_1^l at $(E_1\ , \alpha_1)$ is transferred to a new position (E_2, α_2) through a single interaction with the wave packets, the density f_2^l of the test particle is given by

$$f_2^l(E_2, \alpha_2) = \frac{A(E_1, \alpha_1)}{A(E_2, \alpha_2)}f_1^l(E_1, \alpha_1)\ . \tag{13}$$

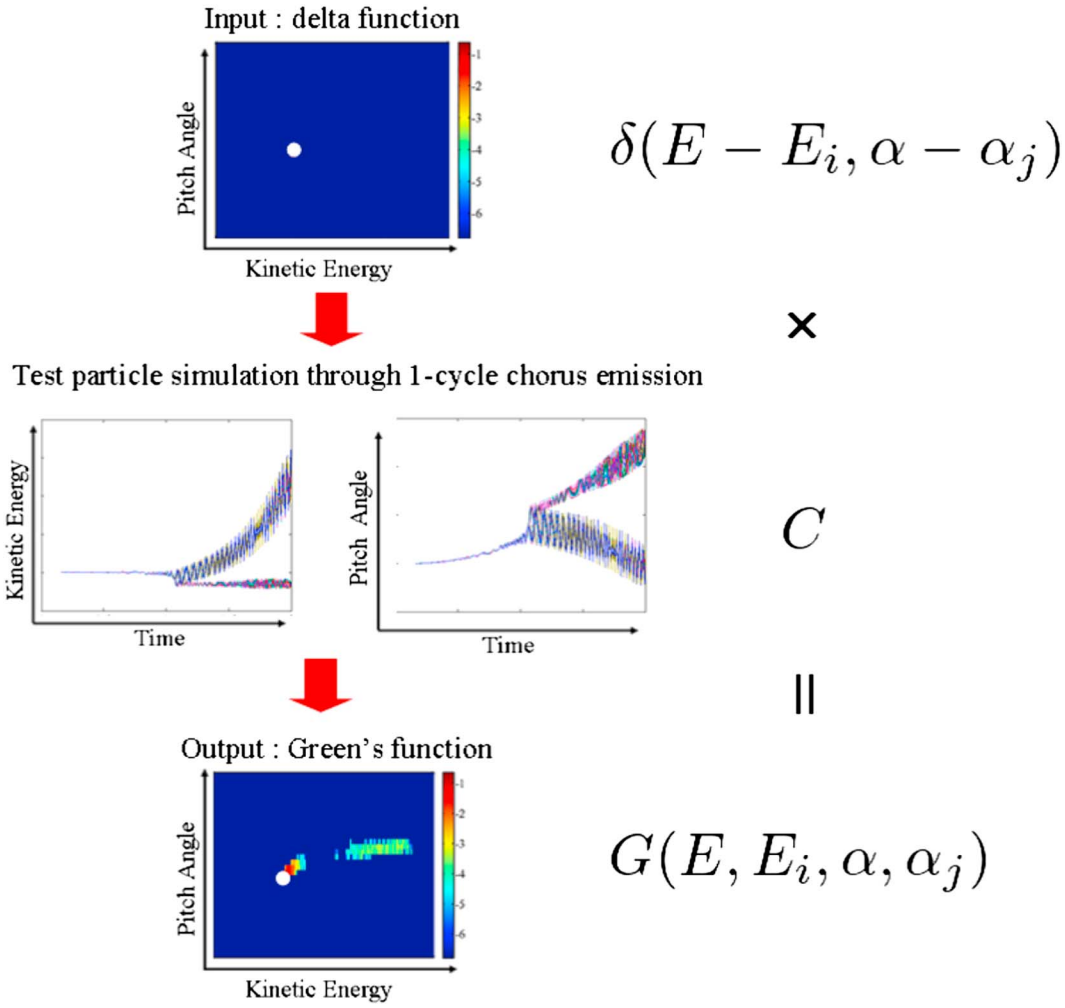

Figure 5. Schematic illustration of the concept for the Green's function method. (top) The initial distribution in energy and equatorial pitch angle. (middle) Trajectories of electrons interacting with a pair of chorus wave packets. (bottom) The Green's function after one cycle of chorus interaction.

We now assume that N_p test particles are located in a small phase space volume $\Delta E \times \Delta\alpha$ around (E_1, α_1) with different positions and gyrophase angle. These test particles are injected at different timings with respect to the propagation of the wave packets. Normalizing the distribution function f_1^l by

$$f_1^l(E_1, \alpha_1) = \frac{1}{N_p \Delta E \Delta\alpha} \ , \tag{14}$$

we then have

$$\sum_{l=1}^{N_p} f_1^l \Delta E \Delta\alpha = 1 \ . \tag{15}$$

By analogy with the definition of the Dirac delta function that satisfies

$$\int\int \delta(E - E_1, \alpha - \alpha_1) \mathrm{d}E \mathrm{d}\alpha = 1 \ , \tag{16}$$

we assume that the group of test particles $\{f_1^l\}$ $(l = 1, 2, 3, ..., N_p)$ forms a Dirac delta function. After scattering by the wave packets, the new distributions of the test particles $\{f_2^l\}$ constitute a Green's function $G(E, E_1, \alpha, \alpha_1)$ which acts as an operator for the chorus wave-particle interactions.

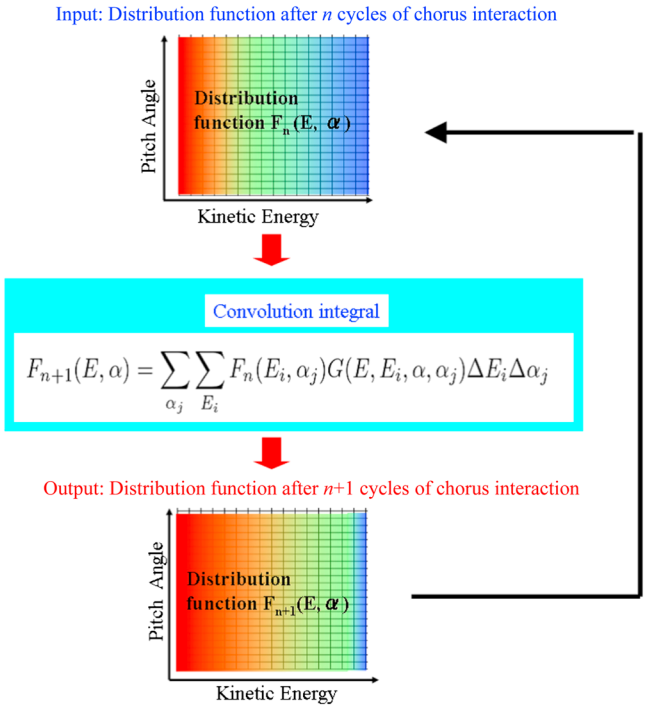

Figure 6. Schematic illustration of the numerical Green's function method for obtaining a long-time evolution of the distribution function $F(E, \alpha)$ of energetic electrons undergoing many cycles of chorus interaction.

After the first cycle of the interaction, the electrons are scattered from the initial location (E_1, α_1) to different energies and pitch angles. We represent this process by the equation

$$G(E, E_1, \alpha, \alpha_1) = C\left[\delta\left(E - E_1, \alpha - \alpha_1\right)\right] \quad . \tag{17}$$

We illustrate the physical meaning of equation (17) in Figure 5. The operator C represents interaction of the group of particles specified by a given argument with the pair of chorus elements described in the previous section. We solve for the trajectories of the electrons numerically using a test particle simulation with the assumed wave model. Since the trajectories of electrons are independent from one another, the operator C has the property of linearity, namely,

$$C[f_a + f_b] = C[f_a] + C[f_b] \tag{18}$$

and

$$wC[f_a] = C[wf_a] \ , \tag{19}$$

where f_a and f_b are arbitrary particle distribution functions and w is a constant. We multiply both sides of (17) by $F_n(E_i, \alpha_j)$, the distribution after n cycles of chorus interaction, and then integrate discretely with respect to energy and equatorial pitch angle. Using equations (18) and (19), we obtain the result

$$\begin{aligned}\sum_{\alpha_j}\sum_{E_i} F_n(E_i,\alpha_j)G(E,E_i,\alpha,\alpha_j)\Delta E_i\Delta\alpha_j &= \sum_{\alpha_j}\sum_{E_i} F_n(E_i,\alpha_j)C[\delta(E-E_i,\alpha-\alpha_j)]\Delta E_i\Delta\alpha_j \\ &= C\left[\sum_{\alpha_j}\sum_{E_i} F_n(E_i,\alpha_j)\delta(E-E_i.\alpha-\alpha_j)\Delta E_i\Delta\alpha_j\right] \\ &= C[F_n(E,\alpha)] = F_{n+1}(E,\alpha) \ .\end{aligned} \tag{20}$$

The right-hand side of (20) corresponds to the distribution function after $n + 1$ cycles of chorus interaction. Thus, we can calculate the distribution function after $n + 1$ cycles by taking the sum of the products of the

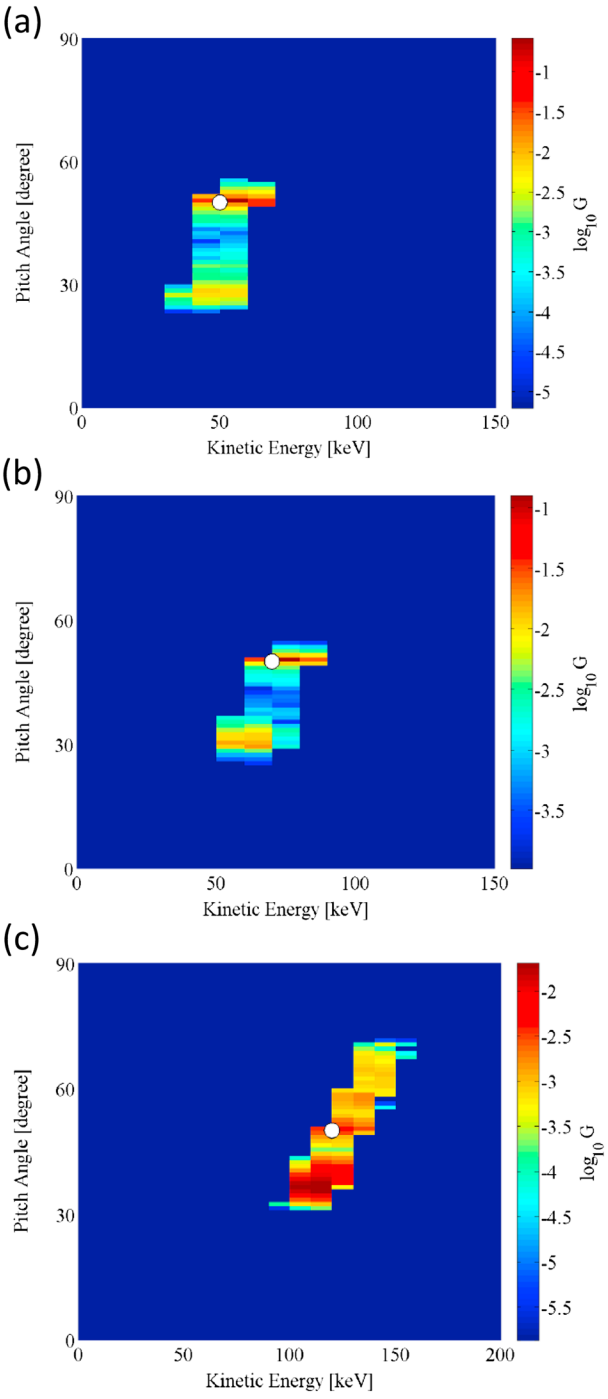

Figure 7. Green's functions after one cycle of chorus interaction at different energies. The initial equatorial pitch angle is 50°, and the initial kinetic energies are (a) 50 keV, (b) 70 keV, and (c) 120 keV. The white dot in each panel shows the initial kinetic energy and equatorial pitch angle.

distribution function after n cycles and the Green's function at each location (E_i, α_j) in the phase space as illustrated in Figure 6. This is equivalent to the convolution integral performed in the mathematical Green's function method. We assume that the initial distribution function F_0 represents a fresh injection of electrons into the equatorial region. After the interaction with a pair of chorus wave packets, we assume that the low-energy part (10–30 keV) of the energetic electron distribution mostly contributing to the generation of chorus emissions is mixed in velocity phase space due to the continuous injection of electrons. The distribution achieves equilibrium along the field line, enabling the generation of another pair of chorus wave packets. By repeating the convolution integral numerically, we can thereby follow a long-time evolution of the distribution function of energetic electrons.

4. Examples of Numerical Green's Functions for Chorus Interaction

We have calculated numerical Green's functions for electron energies from 10 keV to 6 MeV and equatorial pitch angles from 10° to 90°. These ranges correspond to the typical energy and equatorial pitch angle ranges of radiation belt electrons. In calculating each of Green's functions, we use a number of particles $N_p = 3600$ with different combinations of 36 gyrophases, 10 locations between the equator and the mirror point, and 10 injection timings with respect to the propagating wave packets. We set up two-dimensional grids in phase space (E, α) with a resolution of 10 keV and 1°. Based on an area-weighting method used in two-dimensional particle simulations [e.g., *Matsumoto and Omura*, 1985], we count a number of particles on each grid transported from the delta function consisting of N_p particles. By multiplying the number density and the phase space density f_2^l given by (13) and (14), we obtain a Green's function.

As examples, we have plotted Green's functions for the delta functions at a pitch angle of 50° and at kinetic energies 50 keV, 70 keV, and 120 keV in Figures 7a–7c, respectively. Pitch angle scattering mostly takes place

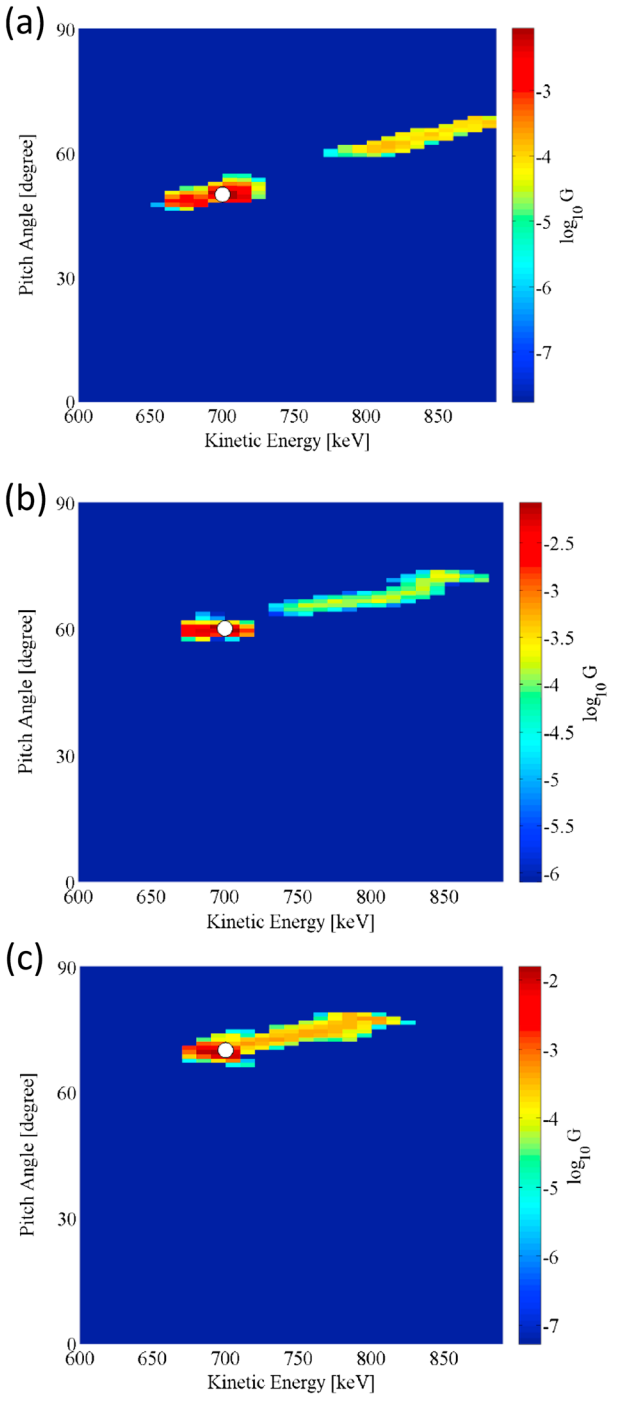

Figure 8. Green's functions after one cycle of chorus interaction at different equatorial pitch angles. The initial kinetic energy is 700 keV, and the initial equatorial pitch angles are (a) 50°, (b) 60°, and (c) 70°.

to lower angles at lower initial energies 50 keV and 70 keV, while at higher-energy 120 keV we find pitch angle scattering to higher angles as well as lower angles. With increasing pitch angles, the kinetic energy also increases as a result of nonlinear trapping by the wave.

In Figures 8a–8c, we plot examples of the Green's function for electrons initially at 700 keV with pitch angles, 50°, 60°, and 70°, respectively. Although the majority of the electrons lose energy by 40 keV at most, some of the electrons are efficiently accelerated by 100–200 keV. In this energy range, the pitch angles increase as the electrons are accelerated because of RTA. The RTA occurs when the energy of resonant electrons is slightly less than 0.51 $(\Omega_e/\omega-1)$ MeV. Some of the resonant electrons moving toward the equator are trapped by the wave potential. Once the electrons are trapped by the wave potentials, they are guided along the resonance velocity, being accelerated efficiently to higher equatorial pitch angles as shown in Figure 8. Trajectories of trapped electrons and those of untrapped electrons become very different, as shown in Figure 2. Eventually, there appears a gap in the Green's function. This gap is due to the transport of electrons by nonlinear wave trapping, which cannot be described by diffusion equations. There are some fluctuations in the appearance of the gaps because of the coarse representation of the delta functions by the limited number (3600) of electrons.

In much higher energy ranges greater than 0.51 $(\Omega_e/\omega - 1)$ MeV, however, the resonance velocity becomes positive in the same direction as the wave propagation. The acceleration by nonlinear wave trapping thus takes place mostly in the parallel direction as a result of URA, in which the resonance velocity approaches the phase velocity, lowering the equatorial pitch angles as shown in Figure 9. Green's functions starting with energy 2 MeV and pitch angles 60°, 70°, and 80° are plotted in Figures 9a–9c, respectively. We find very efficient URA by about 400 keV, and we observe that this acceleration is much greater than RTA. This is because of the longer interaction times of particles moving in the same direction as the wave propagation. Both RTA and URA are acceleration by nonlinear wave trapping. In the URA

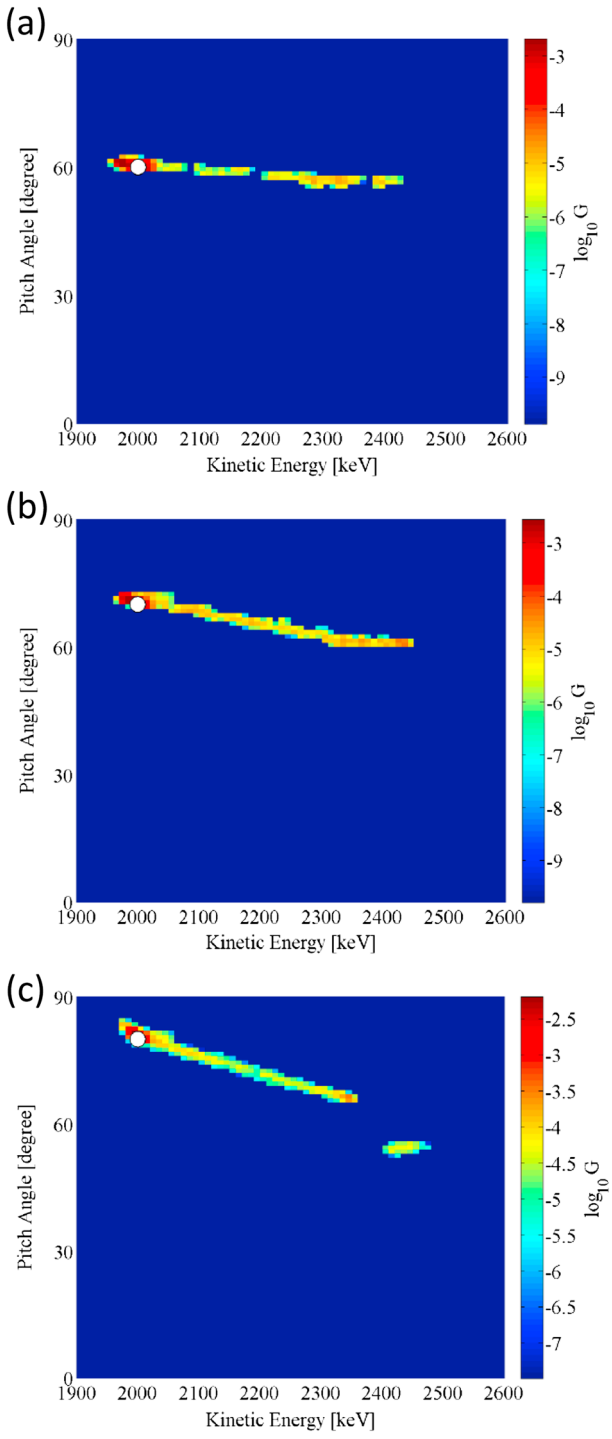

Figure 9. Green's functions after one cycle of chorus interaction at different equatorial pitch angles. The initial kinetic energy is 2.0 MeV, and the initial equatorial pitch angles are (a) 60°, (b) 70°, and (c) 80°.

process, resonant electrons move in the same direction as the wave packet, while RTA starts with resonant electrons moving in the opposite direction to the wave packet.

5. Long-Time Evolution of the Distribution Function

In the previous section, we performed test particle simulations and obtained a set of electron distribution functions evolving from delta functions for the wide range of pitch angles and energies. We calculated

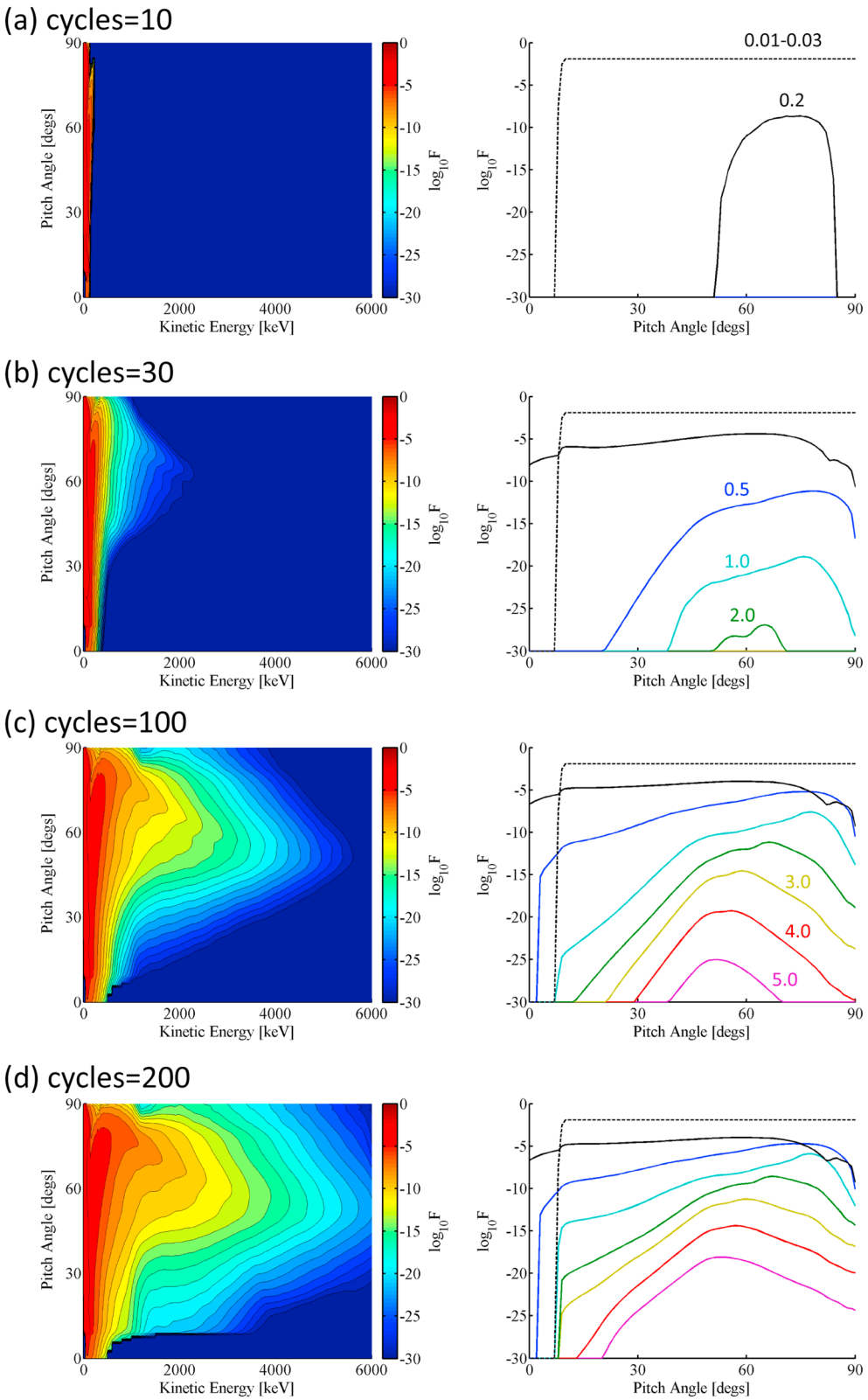

Figure 10. Time evolution of the energetic electron distribution function $F(E, \alpha)$. The initial distribution function $F_0(E, \alpha)$ is set as a stationary distribution with the energy range from 10 keV to 30 keV and the pitch angle range from 10° to 90°. (left column) The $\log_{10} F(E, \alpha)$ after different cycles of interaction are plotted, and (right column) their cross sections at $E = 0.01 - 0.03$ MeV (dashed), 0.2 MeV (black), 0.5 MeV (blue), 1 MeV (cyan), 2 MeV (green), 3 MeV (yellow), 4 MeV (red), and 5 MeV (magenta) are plotted.

Green's functions for the lower energy range 10 keV to 400 keV with an interval $\Delta E = 10$ keV and for equatorial pitch angles (10, 15, 20, ..., 75, 80, 85, 86, 87, 88, 89, and 90°). We have increased the resolution in pitch angles greater than 85° to resolve the fine structures due to the RTA process. For the higher-energy range 400 keV to 6 MeV, we use $\Delta E = 100$ keV, while the resolution of equatorial pitch angle is the same. In order to analyze the shape of the Green's function that is required to change smoothly in the range from keV to MeV, we need to define the Green's functions with a high degree of accuracy in the grids in phase space of kinetic energy and pitch angle. Assuming that shapes of Green's functions vary smoothly with respect to changes in energy and pitch angle, we interpolate the Green's functions by using a linear weighting method to obtain Green's functions with intervals $\Delta E = 10$ keV and $\Delta\alpha = 1°$.

For the initial velocity distribution function, we assume a flat distribution function $F_0(E, \alpha)$ over $E = 10 - 30$ keV and $\alpha = 10° - 90°$. We normalize F_0 so that the integration over E and α becomes unity. To simulate a constant influx of energetic electrons, we maintain the constant distribution during all cycles of chorus interaction. This assumption corresponds to the steady injection of energetic electrons from the tailside into the equatorial region of the inner magnetosphere. We neglect electrons which have equatorial pitch angles less than the loss cone angle of 10°, since such electrons do not remain trapped in the outer radiation belt. We calculate the convolution integrals over every energy and equatorial pitch angle from the loss cone angle to 90°.

We find that the electron distribution function is energized via the chorus emissions very rapidly. The physical parameters are the same as given in section 2 describing the model of chorus emissions. As we see from Figures 10a and 10b, we find the formation of electron flux at high pitch angles > 50°. The equatorial pitch angle α becomes larger within a few tens of chorus interactions in the kinetic energy range $E < 1$ MeV, within which electrons starting from 10 to 30 keV are accelerated gradually by nonlinear trapping. In the low-energy range the acceleration is not significant during the first 10 cycles of interaction, but once the electrons are accelerated to 0.5 MeV or more, the very effective RTA process sets in, and electrons are accelerated toward $\alpha = 90°$.

In Figures 10c and 10d, on the other hand, the equatorial pitch angles of electrons accelerated beyond 1 MeV becomes gradually smaller as the number of chorus interaction cycles increases. After 200 cycles, a substantial flux of relativistic electrons is formed, as shown in Figure 10d. The distribution function of relativistic electrons gradually approaches a constant profile. As shown in the right column of Figure 10, the density of 1 MeV electrons reaches a level of $10^{-4}F_0$ near the equatorial pitch angle 80°, and the density of 5 MeV electrons increases to $10^{-15}F_0$ near 50°. The results suggest that electrons are further accelerated effectively by the URA process, which lowers the pitch angles of trapped resonant electrons, with the parallel velocities increasing toward the phase velocity. The URA mechanism occurs when electrons and the waves are moving in the same direction, and consequently the resonant interaction time becomes longer than that in the RTA process, resulting in very efficient acceleration.

We find that the combined effective acceleration processes of RTA and URA due to the interactions with chorus emissions contribute to the rapid formation of the relativistic electron flux in the outer radiation belt. In order to check the validity of the long-time evolution of the distribution function, we estimate the resonance region in phase space of kinetic energy and equatorial pitch angle. The resonance velocity V_R and the perpendicular component $v_\perp$ of the electron velocity are given by

$$V_R = \frac{\omega - \Omega_e/\gamma}{k} \tag{21}$$

and

$$v_\perp = V_R \tan\alpha \ , \tag{22}$$

where ω and k are wave frequency and wave number of a chorus element. The Lorentz factor γ is expressed as

$$\gamma = \frac{1}{\sqrt{1 - \left(V_R{}^2 + v_\perp{}^2\right)/c^2}} \ . \tag{23}$$

Using (21)–(23), we obtain the relation between Lorentz factor γ and the pitch angle α as

$$\sin^2\alpha = 1 - \left(\frac{\omega}{ck}\right)^2 \frac{(\gamma - \Omega_e/\omega)^2}{\gamma^2 - 1} \ . \tag{24}$$

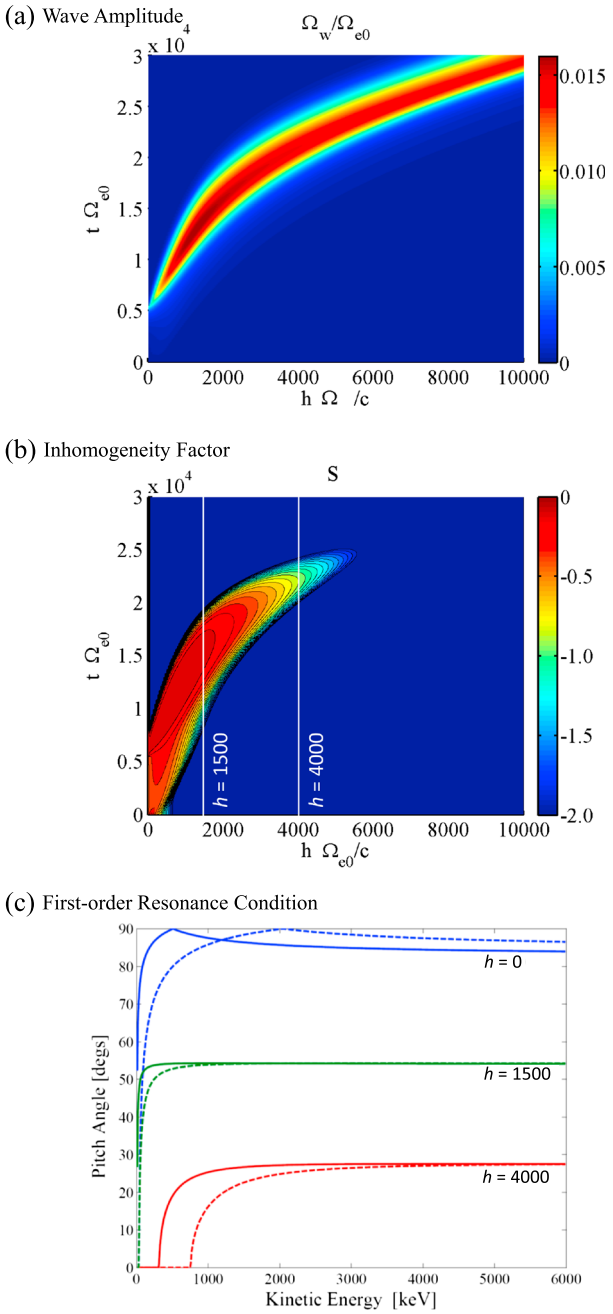

Figure 11. (a) Evolution of the amplitude of the chorus wave packet in the Northern Hemisphere during one cycle of chorus interaction $t\Omega_{e0} = 0 - 30{,}000$. (b) Spatial and temporal variation of the inhomogeneity factor S of electrons with the average perpendicular velocity $V_{\perp 0} = 0.3c$. (c) The first-order resonance conditions at $h\Omega_{e0}/c = 0$ (blue), 1500 (green), and 4000 (red) are plotted for $\omega/\Omega_{e0} = 0.2$ and 0.5 as dashed and solid lines, respectively.

Assuming adiabatic motion, we convert the pitch angle α at a distance h to the equatorial pitch angle α_{eq} by using

$$\sin \alpha_{eq} = \left\{ \frac{\Omega_{e0}}{\Omega_e(h)} \left[1 - \frac{\beta\omega^2}{\omega_{pe}^2(h) + \beta\omega^2} \frac{(\beta - \tilde{E})^2}{\tilde{E}(\tilde{E} + 2)} \right] \right\}^{1/2}, \tag{25}$$

where $\beta = \Omega_e(h)/\omega - 1$, $\tilde{E} = E/(m_e c^2) = \gamma - 1$, and $\Omega_e(h)$ and $\omega_{pe}(h)$ are the local cyclotron frequency and plasma frequency, respectively. The equatorial pitch angle is now expressed as a function of the kinetic energy E of resonant electrons interacting with a whistler-mode wave of frequency ω.

Figure 11a shows an amplitude profile of the chorus wave packet in the Northern Hemisphere throughout the test particle simulation involving the calculation of Green's functions. In order to determine the range of the spatial width in which electrons can be accelerated effectively through nonlinear wave trapping, we need to calculate the inhomogeneity factor S. This calculation is described in Appendix A. Figure 11b shows the time evolution and spatial profile of the inhomogeneity factor S of resonant electrons with an average perpendicular velocity $V_{\perp 0} = 0.3\,c$. Resonant electrons can be trapped by the nonlinear wave potential when $|S| < 1$. We find that $|S| < 1$ in the spatial range $h = 0 - 4000\,c/\Omega_{e0}$.

The range of kinetic energy and equatorial pitch angle over which electrons can resonate with the waves is obtained by substituting $\omega = 0.2\,\Omega_{e0}$ and $\omega = 0.5\,\Omega_{e0}$ into equation (25). Figure 11c shows the solutions of (25) at $h = 0$ and $4000\,c/\Omega_{e0}$ in blue and red, respectively. The solutions for $\omega = 0.2\ \Omega_{e0}$ and $\omega = 0.5\ \Omega_{e0}$ are plotted in dashed and solid lines, respectively. We also plot the resonance conditions at $h = 1500\,c/\Omega_{e0}$ corresponding to a small value of $|S|$ in green to indicate a region where a larger number of electrons can be trapped by the nonlinear wave potential.

The range of acceleration taking place in the electron distribution function in Figure 10d agrees with the resonance range satisfying $|S| < 1$, as shown in Figures 11b and 11c. When the kinetic energy is less than 0.5 MeV, the resonance region occupies almost all of the pitch angles. As we find in Figure 10d, electrons with pitch angles greater than 10° are effectively scattered to the lower pitch angles by Green's functions defined over this pitch angle range (≥10°). Strong precipitation takes place especially below 0.2 MeV. On the other hand, chorus emissions cannot cause the precipitation of relativistic electrons of a few MeV, since there is no pitch angle scattering to lower angles at 10° above 1.5 MeV in Figure 10d.

6. Summary and Discussion

We have developed a new method of modeling the formation process of the relativistic electron flux due to nonlinear wave-particle interactions with whistler mode chorus emissions. We first construct a chorus wave model in which a pair of chorus elements with rising tone frequencies ($0.2 - 0.5\Omega_{e0}$) are generated at the equator and propagate to higher latitudes. We then calculate trajectories of a large number of electrons with the same initial kinetic energy and equatorial pitch angle, but with different positions and injection timings with respect to the propagation of the chorus wave packets. These electrons are scattered to different energies and equatorial pitch angles due to cyclotron resonance with the waves. Assuming the initial distribution as a delta function, we can obtain the distribution function of the scattered electrons as a Green's function. We calculate a set of Green's functions for different kinetic energies 10 keV − 6 MeV and all pitch angles greater than the loss cone angle. In the calculation of the Green's functions, we have confirmed the very efficient acceleration processes RTA and URA by the nonlinear trapping of resonant electrons. Assuming an injection of 10 − 30 keV electrons, we take the convolution integral with the Green's functions. A one-time convolution integral corresponds to an interaction with a pair of chorus elements propagating northward and southward from the equator. By repeating the convolution integral, we can then follow a long-time evolution of the distribution function of the relativistic electrons interacting with many chorus elements. Formation of the relativistic electron flux (2 ∼ 6 MeV) takes place within a few minutes.

A flux of relativistic electrons is formed at the equatorial pitch angles 50–80° as a result of the RTA process followed by URA. The relativistic electrons (2 − 6 MeV) accelerated by chorus emissions form a dumbbell distribution [*Morioka et al.*, 2001]. If we assume that an occurrence rate of chorus emissions is one pair of chorus emissions per second, then electrons can be accelerated from 30 keV to 6 MeV within 3 min. Quasi-linear diffusion models cannot typically explain such a rapid acceleration. Simulations hitherto published in the literature [e.g., *Horne et al.*, 2005; *Varotsou et al.*, 2005; *Thorne et al.*, 2013; *Li et al.*, 2014] of local electron acceleration by chorus using a Fokker-Planck equation do not represent the real nonlinear physical processes generating chorus emissions and the associated acceleration involving the nonlinear trapping mechanisms RTA and URA.

The numerical method reported in this paper is the first long-timescale modeling of relativistic electron flux in the radiation belts that takes into account these nonlinear mechanisms. In the present study, we assume that chorus emissions propagate purely parallel to the magnetic field. The wave normal angle of a chorus emission, however, becomes gradually oblique as it propagates away from the equator. Landau resonance with a parallel electric field can contribute to the further acceleration of relativistic electrons [*Nunn and Omura*, 2015]. Calculation of Green's functions with obliquely propagating waves is left as a future study.

Appendix A: Inhomogeneity Factor *S*

The dynamics of a resonant electron interacting with a whistler mode wave can be expressed by the set of equations

$$\frac{d\zeta}{dt} = \theta \tag{A1}$$

and

$$\frac{d\theta}{dt} = \omega_{tr}^2(\sin\zeta + S) \ , \tag{A2}$$

with $\omega_{tr} = \omega_t \chi \gamma^{-1/2}$, where ζ is the gyrophase angle with respect to the wave magnetic field, and $\theta = k(v_{\parallel} - V_R)$ is the normalized difference between the parallel velocity and the resonance velocity. We assume that $v_{\parallel} \sim V_R$, i.e., $\theta \sim 0$. Here ω_t is the trapping frequency given by $\omega_t = \sqrt{kv_{\perp}\Omega_w}$. The shape of the electron hole is determined by the inhomogeneity factor *S* given by

$$S = -\frac{1}{s_0 \omega \Omega_w}\left(s_1 \frac{\partial \omega}{\partial t} + c s_2 \frac{\partial \Omega_e}{\partial h}\right) \ , \tag{A3}$$

where

$$s_0 = \frac{\chi}{\xi}\tilde{V}_{\perp 0} \ , \tag{A4}$$

$$s_1 = \gamma(1 - \frac{\tilde{V}_R}{\tilde{V}_g})^2 \ , \tag{A5}$$

and

$$s_2 = \frac{1}{2\xi\chi}\left\{\frac{\gamma\omega}{\Omega_e}\tilde{V}_{\perp 0}^2 - \left[2 + \frac{\chi^2(\Omega_e - \gamma\omega)}{\Omega_e - \omega}\right]\tilde{V}_R\tilde{V}_p\right\} \ . \tag{A6}$$

In defining these variables, we have introduced the dimensionless parameters χ and ξ defined by

$$\chi^2 = 1 - \frac{\omega^2}{c^2k^2} \tag{A7}$$

and

$$\xi^2 = \frac{\omega(\Omega_e - \omega)}{\omega_{pe}^2} \ . \tag{A8}$$

The cold plasma dispersion relation is written as

$$\chi^2 = \frac{1}{1 + \xi^2} \ . \tag{A9}$$

The phase velocity $V_p = \omega/k$, the resonance velocity V_R, and the group velocity $V_g = \partial\omega/\partial k$ are given by the respective equations [*Omura et al.*, 2008, 2012]

$$\tilde{V}_p = V_p/c = \chi\xi \ , \tag{A10}$$

$$\tilde{V}_R = V_R/c = -\chi\xi\left(\frac{\Omega_e}{\gamma\omega} - 1\right) \ , \tag{A11}$$

and

$$\tilde{V}_g = V_g/c = \frac{\xi}{\chi}\left[\xi^2 + \frac{\Omega_e}{2(\Omega_e - \omega)}\right]^{-1} \ , \tag{A12}$$

where we assume $V_p > 0$ with $k > 0$. We also assume the perpendicular velocity $\tilde{V}_{\perp 0} = V_{\perp 0}/c = 0.3$ throughout the present investigation.

Acknowledgments
All the new data used in this paper are obtained from numerical integration of the equations of motion of energetic electrons and calculation of the electron distribution functions by equations (12), (13), and (20). Computations in the present study were performed on the KDK system of the Research Institute for Sustainable Humanosphere (RISH) at Kyoto University. This work was supported by JSPS KAKENHI grants 26287120 and 15H03732. D.S. acknowledges support from a Discovery grant of the Natural Sciences and Engineering Research Council of Canada.

References

Boynton, R. J., M. A. Balikhin, and D. Mourenas (2014), Statistical analysis of electron lifetimes at GEO: Comparisons with chorus-driven losses, *J. Geophys. Res. Space Physics*, *119*, 6356–6366, doi:10.1002/2014JA019920.

Furuya, N., Y. Omura, and D. Summers (2008), Relativistic turning acceleration of radiation belt electrons by whistler mode chorus, *J. Geophys. Res.*, *113*, A04224, doi:10.1029/2007JA012478.

Harid, V., M. Gołkowski, T. Bell, and U. S. Inan (2014), Theoretical and numerical analysis of radiation belt electron precipitation by coherent whistler mode waves, *J. Geophys. Res. Space Physics*, *119*, 4370–4388, doi:10.1002/2014JA019809.

Hikishima, M., S. Yagitani, Y. Omura, and I. Nagano (2009), Full particle simulation of whistler-mode rising chorus emissions in the magnetosphere, *J. Geophys. Res.*, *114*, A01203, doi:10.1029/2008JA013625.

Hikishima, M., Y. Omura, and D. Summers (2010a), Microburst precipitation of energetic electrons associated with chorus wave generation, *Geophys. Res. Lett.*, *37*, L07103, doi:10.1029/2010GL042678.

Hikishima, M., Y. Omura, and D. Summers (2010b), Self-consistent particle simulation of whistler-mode triggered emissions, *J. Geophys. Res.*, *115*, A12246, doi:10.1029/2010JA015860.

Horne, R. B., R. M. Thorne, S. A. Glauert, J. M. Albert, N. P. Meredith, and R. R. Anderson (2005), Timescale for radiation belt electron acceleration by whistler mode chorus waves, *J. Geophys. Res.*, *110*, A03225, doi:10.1029/2004JA00811.

Jordanova, V. K., L. M. Kistler, J. U. Kozyra, G. V. Khazanov, and A. F. Nagy (1996), Collisional losses of ring current ions, *J. Geophys. Res.*, *101*(A1), 111–126, doi:10.1029/95JA02000.

Katoh, Y., and Y. Omura (2007a), Computer simulation of chorus wave generation in the Earth's inner magnetosphere, *Geophys. Res. Lett.*, *34*, L03102, doi:10.1029/2006GL028594.

Katoh, Y., and Y. Omura (2007b), Relativistic particle acceleration in the process of whistler-mode chorus wave generation, *Geophys. Res. Lett.*, *34*, L13102, doi:10.1029/2007GL029758.

Koons, H. C., and J. L. Roeder (1990), A survey of equatorial magnetospheric wave activity between 5 and 8 R_E, *Planet. Space Sci.*, *38*, 1335–1341.

Lakhina, G. S., B. T. Tsurutani, O. P. Verkhoglyadova, and J. S. Pickett (2010), Pitch angle transport of electrons due to cyclotron interactions with the coherent chorus subelements, *J. Geophys. Res.*, *115*, A00F15, doi:10.1029/2009JA014885.

Li, W., et al. (2014), Radiation belt electron acceleration by chorus waves during the 17 March 2013 storm, *J. Geophys. Res. Space Physics*, *119*, 4681–4693, doi:10.1002/2014JA019945.

Liu, S., et al. (2015), Van Allen Probes observations linking radiation belt electrons to chorus waves during 2014 multiple storms, *J. Geophys. Res. Space Physics*, *120*, 938–948, doi:10.1002/2014JA020781.

Lorentzen, K. R., J. B. Blake, U. S. Inan, and J. Bortnik (2001), Observations of relativistic electron microbursts in association with VLF chorus, *J. Geophys. Res.*, *106*, 6017–6027.

Matsumoto, H., and Y. Omura (1985), Particle simulations of electromagnetic waves and its applications to space plasmas, in *Computer Simulations of Space Plasmas*, edited by H. Matsumoto and T. Sato, pp. 43–102, Terra Sci. and D. Reidel, Tokyo and Dordrecht.

Meredith, N. P., R. B. Horne, and R. R. Anderson (2001), Substorm dependence of chorus amplitudes: Implications for the acceleration of electrons to relativistic energies, *J. Geophys. Res.*, *106*, 13,165–13,178.

Meredith, N. P., R. B. Horne, W. Li, R. M. Thorne, and A. Sicard-Piet (2014), Global model of low-frequency chorus ($f_{LHR} < f < 0.1f_{ce}$) from multiple satellite observations, *Geophys. Res. Lett.*, *41*, 280–286, doi:10.1002/2013GL059050.

Mourenas, D., A. Artemyev, O. Agapitov, and V. Krasnoselskikh (2012), Acceleration of radiation belts electrons by oblique chorus waves, *J. Geophys. Res.*, *117*, A10212, doi:10.1029/2012JA018041.

Morioka, A., H. Misawa, Y. Miyoshi, H. Oya, M. Iijima, and T. Nagai (2001), Pitch angle distribution of relativistic electrons in the inner radiation belt and its relation to equatorial plasma wave turbulence phenomena, *Geophys. Res. Lett.*, *28*, 931–934, doi:10.1029/2000GL011886.

Nunn, D., and Y. Omura (2015), A computational and theoretical investigation of nonlinear wave-particle interactions in oblique whistlers, *J. Geophys. Res. Space Physics*, *120*, 2890–2911, doi:10.1002/2014JA020898.

Nunn, D., Y. Omura, H. Matsumoto, I. Nagano, and S. Yagitani (1997), The numerical simulation of VLF chorus and discrete emissions observed on the Geotail satellite using a Vlasov code, *J. Geophys. Res.*, *102*, 27,083–27,097.

O'Brien, T. P., M. D. Looper, and J. B. Blake (2004), Quantification of relativistic electron microburst losses during the GEM storms, *Geophys. Res. Lett.*, *31*, L04802, doi:10.1029/2003GL018621.

Omura, Y., and D. Summers (2006), Dynamics of high-energy electrons interacting with whistler mode chorus emissions in the magnetosphere, *J. Geophys. Res.*, *111*, A09222, doi:10.1029/2006JA011600.

Omura, Y., D. Nunn, H. Matsumoto, and M. J. Rycroft (1991), A review of observational, theoretical and numerical studies of VLF triggered emissions, *J. Atmos. Terr. Phys.*, *53*, 351–368.

Omura, Y., N. Furuya, and D. Summers (2007), Relativistic turning acceleration of resonant electrons by coherent whistler mode waves in a dipole magnetic field, *J. Geophys. Res.*, *112*, A06236, doi:10.1029/2006JA012243.

Omura, Y., Y. Katoh, and D. Summers (2008), Theory and simulation of the generation of whistler-mode chorus, *J. Geophys. Res.*, *113*, A04223, doi:10.1029/2007JA012622.

Omura, Y., M. Hikishima, Y. Katoh, D. Summers, and S. Yagitani (2009), Nonlinear mechanisms of lower-band and upper-band VLF chorus emissions in the magnetosphere, *J. Geophys. Res.*, *114*, A07217, doi:10.1029/2009JA014206.

Omura, Y., D. Nunn, and D. Summers (2012), Generation processes of whistler mode chorus emissions: Current status of nonlinear wave growth theory, in *Dynamics of the Earth's Radiation Belts and Inner Magnetosphere, Geophys. Monogr. Ser.*, vol. 199, edited by D. Summers, pp. 243–254, AGU, Washington, D. C., doi:10.1029/2012GM001347.

Santolik, O., E. Macusova, E. E. Titova, B. V. Kozelov, D. A. Gurnett, J. S. Pickett, V. Y. Trakhtengerts, and A. G. Demekhov (2008), Frequencies of wave packets of whistler-mode chorus inside its source region: A case study, *Ann. Geophys.*, *26*, 1665–1670.

Santolik, O., C. A. Kletzing, W. S. Kurth, G. B. Hospodarsky, and S. R. Bounds (2014), Fine structure of large amplitude chorus waves packets, *Geophy. Res. Lett.*, *41*, 293–299, doi:10.1002/2013GL058889.

Spasojevic, M. (2014), Statistical analysis of ground-based chorus observations during geomagnetic storms, *J. Geophys. Res. Space Physics*, *119*, 8299–8317, doi:10.1002/2014JA019975.

Shprits, Y. Y., N. P. Meredith, and R. M. Thorne (2007), Parameterization of radiation belt electron loss timescales due to interactions with chorus waves, *Geophys. Res. Lett.*, *34*, L11110, doi:10.1029/2006GL029050.

Su, Z., et al. (2014), Intense duskside lower-band chorus waves observed by Van Allen Probes: Generation and potential acceleration effect on radiation belt electrons, *Geophys. Res. Lett.*, *119*, 4266–4273, doi:10.1002/2014JA019919.

Summers, D., and Y. Omura (2007), Ultra-relativistic acceleration of electrons in planetary magnetospheres, *Geophys. Res. Lett.*, *34*, L24205, doi:10.1029/2007GL032226.

Summers, D., and R. Shi (2014), Limiting energy spectrum of an electron radiation belt, *J. Geophys. Res. Space Physics*, *119*, 6313–6326, doi:10.1002/2014JA020250.

Summers, D., R. M. Thorne, and F. Xiao (1998), Relativistic theory of wave-particle resonant diffusion with application to electron acceleration in the magnetosphere, *J. Geophys. Res.*, *103*, 20,487–20,500, doi:10.1029/98JA01740.

Summers, D., C. Ma, N. P. Meredith, R. B. Horne, R. M. Thorne, D. Heynderickx, and R. R. Anderson (2002), Model of the energization of outer-zone electrons by whistler-mode chorus during the October 9, 1990 geomagnetic storm, *Geophys. Res. Lett.*, *29*(24), 2174, doi:10.1029/2002GL016039.

Summers, D., B. Ni, and N. P. Meredith (2007), Timescales for radiation belt electron acceleration and loss due to resonant wave-particle interactions: 2. Evaluation for VLF chorus, ELF hiss, and electromagnetic ion cyclotron waves, *J. Geophys. Res.*, *112*, A04207, doi:10.1029/2006JA011993.

Summers, D., R. Tang, and R. M. Thorne (2009), Limit on stably trapped particle fluxes in planetary magnetospheres, *J. Geophys. Res.*, *114*, A10210, doi:10.1029/2009JA014428.

Summers, D., Y. Omura, Y. Miyashita, and D.-H. Lee (2012), Nonlinear spatio-temporal evolution of whistler mode chorus waves in Earth's inner magnetosphere, *J. Geophys. Res.*, *117*, A09206, doi:10.1029/2012JA017842.

Thorne, R. M., T. P. O'Brien, Y. Y. Shprits, D. Summers, and R. B. Horne (2005), Timescale for MeV electron microburst loss during geomagnetic storms, *J. Geophys. Res.*, *110*, A09202, doi:10.1029/2004JA010882.

Thorne, R. M., et al. (2013), Rapid local acceleration of relativistic radiation-belt electrons by magnetospheric chorus, *Nature*, *504*, 411–414.

Tsurutani, B. T., and E. J. Smith (1974), Postmidnight chorus: A substorm phenomenon, *J. Geophys. Res.*, *79*, 118–127.

Tsurutani, B. T., O. P. Verkhoglyadova, G. S. Lakhina, and S. Yagitani (2009), Properties of dayside outer zone chorus during HILDCAA events: Loss of energetic electrons, *J. Geophys. Res.*, *114*, A03207, doi:10.1029/2008JA013353.

Varotsou, A., D. Boscher, S. Bourdarie, R. B. Horne, S. A. Glauert, and N. P. Meredith (2005), Simulation of the outer radiation belt electrons near geosynchronous orbit including both radial diffusion and resonant interaction with whistler-mode chorus waves, *Geophys. Res. Lett.*, *32*, L19106, doi:10.1029/2005GL023282.

Xiao, F., et al. (2014), Chorus acceleration of radiation belt relativistic electrons during March 2013 geomagnetic storm, *J. Geophys. Res. Space Physics*, *119*, 3325–3332, doi:10.1002/2014JA019822.